
This manuscript is a pre-print and has been submitted for publication in PROCEEDINGS OF THE NATIONAL ACADEMY OF SCIENCES (PNAS). Subsequent versions of this manuscript may have slightly different content. If accepted, the final version of this manuscript will be available via the *'Peer-reviewed Publication DOI'* link on the top of this webpage. Please feel free to contact any of the authors; we welcome feedback.

1 **High rates of rock organic carbon oxidation sustained as Andean sediment**
2 **transits the Amazon foreland-floodplain**

3
4 Mathieu Dellinger^{1,2*}, Robert G. Hilton^{1,3}, Mark A. Torres⁴, Emily I. Burt⁵, J. Jotautas
5 Baronas⁶, Kasey E. Clark⁷, Valier Galy⁸, Adan Julian Ccahuana Quispe⁹, A. Joshua West⁵
6

7 ¹ Department of Geography, Durham University, Durham, DH1 3LE, UK

8 ² EDYTEM-CNRS-University Savoie Mont Blanc (USMB), Chambéry, 73000, France

9 ³ Department of Earth Sciences, University of Oxford, Oxford, OX1 3AN, UK

10 ⁴ Department of Earth, Environmental, and Planetary Sciences, Rice University, Houston, TX,
11 USA

12 ⁵ Department of Earth Sciences, University of Southern California (USC), Los Angeles, CA,
13 90089, USA

14 ⁶ Université de Paris, Institut de physique du globe de Paris, CNRS, F-75005, Paris, France

15 ⁷ Department of Geography & Planning, University of Liverpool, Roxby Building, Liverpool,
16 L69 7ZT, UK

17 ⁸ Department of Marine Chemistry and Geochemistry, Woods Hole Oceanographic Institution,
18 Woods Hole, MA, 02543, USA

19 ⁹ Escuela Profesional de Biología, Facultad de Ciencias, Universidad Nacional de San Antonio
20 Abad del Cusco, Cusco 08000, Peru

21
22 ***Email:** mathieu.dellinger@univ-smb.fr
23

24 **Author Contributions:**

25 MD, RGH and AJW designed the research and obtained funding. All authors contributed to
26 fieldwork and sample collection. MD undertook the geochemical analysis of materials for this
27 work. MD analyzed and interpreted the data with RGH. MD and RGH wrote the manuscript
28 with input from all authors.
29

30 **Competing Interest Statement:**

31 The authors declare no competing interests.
32

33 **Classification:**

34 Earth, Atmospheric, and Planetary Sciences
35

36 **Keywords:**

37 Carbon cycle; weathering; rivers; Amazon; Andes; Organic carbon
38
39
40

41 **Abstract**

42 The oxidation of organic carbon contained within sedimentary rocks (“petrogenic” carbon, or
43 hereafter OC_{petro}) emits nearly as much CO_2 as is released by volcanism, thereby playing a key
44 role in the long-term global C budget. High erosion rates in mountains have been shown to
45 increase OC_{petro} oxidation. However, these settings also export un-weathered material that may
46 continue to react in downstream floodplains. The relative importance of OC_{petro} oxidation in
47 mountains versus floodplains remains difficult to assess as disparate methods have been used
48 in the different environments. Here, we investigate the sources and fluxes of rhenium (Re) in
49 the Rio Madre de Dios to quantify OC_{petro} oxidation from the Andes to the Amazon floodplains
50 using a common approach. Dissolved rhenium concentrations ($n=131$) range from 0.01 to 63
51 pmol.L^{-1} and vary depending on lithology and geomorphic setting. We find that $>75\%$ of the
52 dissolved Re derives from OC_{petro} oxidation and that this proportion increases downstream. We
53 estimate that in the Andes, OC_{petro} oxidation releases $11.2^{+4.5}_{-2.8} \text{ tC km}^{-2} \text{ yr}^{-1}$ of CO_2 , which
54 corresponds to $\sim 40\%$ of the total OC_{petro} denudation. A Re mass balance across the Rio Madre
55 de Dios shows that 46% of OC_{petro} oxidation takes place in the Andes, 14% in the foreland-
56 lowlands, and 40% in the Andean-fed floodplains. This doubling of OC_{petro} oxidation flux
57 downstream of the Andes demonstrates that floodplains can greatly increase OC_{petro} oxidation
58 and CO_2 release associated with mountain building, further tipping these landscapes towards
59 being a source of CO_2 .

61 **Significance Statement:**

62 Erosion and weathering play key roles in Earth’s carbon cycle, controlling climate over millions
63 of years by transferring CO_2 to and from the atmosphere. Weathering of sedimentary rocks
64 releases CO_2 through petrogenic organic carbon oxidation and previous work has shown that
65 mountains are CO_2 hotspots release. However, a large amount of petrogenic organic carbon
66 survives oxidation in mountains and is transported through river floodplains to an unknown
67 fate. Here we use rhenium to quantify oxidative weathering in the eastern Andes Mountains
68 and adjacent Amazon floodplain. Erosion in the Andes leads to high rates of CO_2 release.
69 However, CO_2 release doubles when including the foreland-floodplains. Geomorphic setting
70 governs CO_2 release by oxidative weathering and whether catchments act as CO_2 sources.

72 **Main text:**

74 **Introduction**

75 Substantial climatic changes have occurred throughout geologic time, with the evolution of the
76 carbon cycle and the planet’s habitability modulated by the interplay between tectonic, climatic,
77 erosional and biological processes. Over long timescales ($>10^5$ years), the abundance of CO_2
78 in the atmosphere is determined by the balance of the major carbon sources and sinks (1). It has
79 been widely debated how the Earth system responds to transient imbalances in the long-term
80 carbon (C) cycle, with much focus of prior research on the CO_2 sink associated with the
81 chemical weathering of silicate minerals (1, 2). However, recent studies have highlighted the
82 potential importance of changes in CO_2 fluxes linked to oxidative weathering (OW) reactions
83 of sedimentary rocks on the continents (3–5). Although receiving less attention to date, OW of
84 reduced phases in sedimentary rocks is central to both the C and O cycles (6, 7). Carbon dioxide
85 release and O_2 consumption can result from both (i) oxidation of fossil (i.e. “rock-derived” or
86 “petrogenic”) organic matter (OC_{petro}) and (ii) the OW of sulfides that produces sulfuric acid,
87 which can be neutralized by carbonate minerals, or by the carbonate buffer of continental waters
88 leading to net CO_2 release to the atmosphere (8, 9).

89 The export of particulate OC_{petro} by rivers in their sediment load has been documented
90 in many places (10–16), but only a few field-based studies have estimated the rate of OW of
91 OC_{petro} (3). The highest fluxes of OC_{petro} oxidation (reported as a yield per catchment area, of 5
92 to $30 \text{ tC.km}^{-2}.\text{yr}^{-1}$) have been measured in small high standing islands composed of sedimentary
93 rocks such as in Taiwan (17) and the New Zealand Southern Alps (4), as well as in catchments
94 from major mountain ranges (0.5 to $5 \text{ tC.km}^{-2}.\text{yr}^{-1}$) like the Yamuna (18), Swiss Alps (19) and
95 in the Mackenzie River basin (20). This reflects the role of physical erosion rate in mountains
96 that can continuously supply OC_{petro} to oxygenated surface waters and the atmosphere (17, 21).
97 A consequence is that, in combination with carbonate weathering by sulfuric acid, CO_2 release
98 by OC_{petro} oxidation can be larger than CO_2 consumption by silicate weathering in many erosive
99 settings (3), challenging the idea that chemical weathering in mountain belts is a long-term
100 carbon sink (22, 23).

101 While physical erosion can enhance the supply of reduced phases to OW reactions and
102 increase the weathering flux (8, 17, 24), the overall intensity of weathering can also decline
103 (25), meaning that erosive catchments can also export very large amounts of ‘unweathered’
104 particulate OC_{petro} (7). These particulate fluxes can be very high, for instance reaching 250
105 $\text{tC.km}^{-2}.\text{yr}^{-1}$ (13, 25). The subsequent fate of this material is critical to governing how physical
106 erosion and weathering impact the carbon cycle. It has been proposed (10, 14) that this OC_{petro}
107 can be largely oxidized in floodplains when present (e.g. in the Amazon and Ganges
108 floodplain), because of the long residence time of sediments and the warm and oxidative
109 conditions that prevail in the floodplains relative to upstream mountainous area. Hence, the
110 combination of mountain catchments underlain by sedimentary rocks with river floodplains
111 could largely enhance the net CO_2 release from OW.

112 Despite the recognition of these geomorphological controls on OW (3), the relative
113 contributions of mountain versus floodplain weathering to OC_{petro} oxidation and CO_2 release
114 remains unknown. This knowledge gap arises in part because different methods have been used
115 to assess OC_{petro} oxidation in mountain catchments (4, 17) versus floodplains (10, 14). In
116 mountain catchments, dissolved rhenium (Re) fluxes have been used as a proxy for quantifying
117 OC_{petro} oxidation fluxes (17), whereas studies on floodplains have used sediment fluxes and the
118 differences in the radiocarbon content of river sediments upstream and downstream (Bouchez
119 et al., 2010). Both methods have benefits and drawbacks. Dissolved Re fluxes are easier to
120 measure because water discharge is usually known with more precision than sediment flux. On
121 the other hand, there are large uncertainties on the source of dissolved Re and on the estimation
122 of the Re/ OC_{petro} ratio of the bedrock (20). Finally, because water and sediments integrate over
123 different spatial and temporal scales, their direct comparison can be problematic. Overall, the
124 influence of floodplains on the global OC_{petro} budget remains an open question (3, 26).

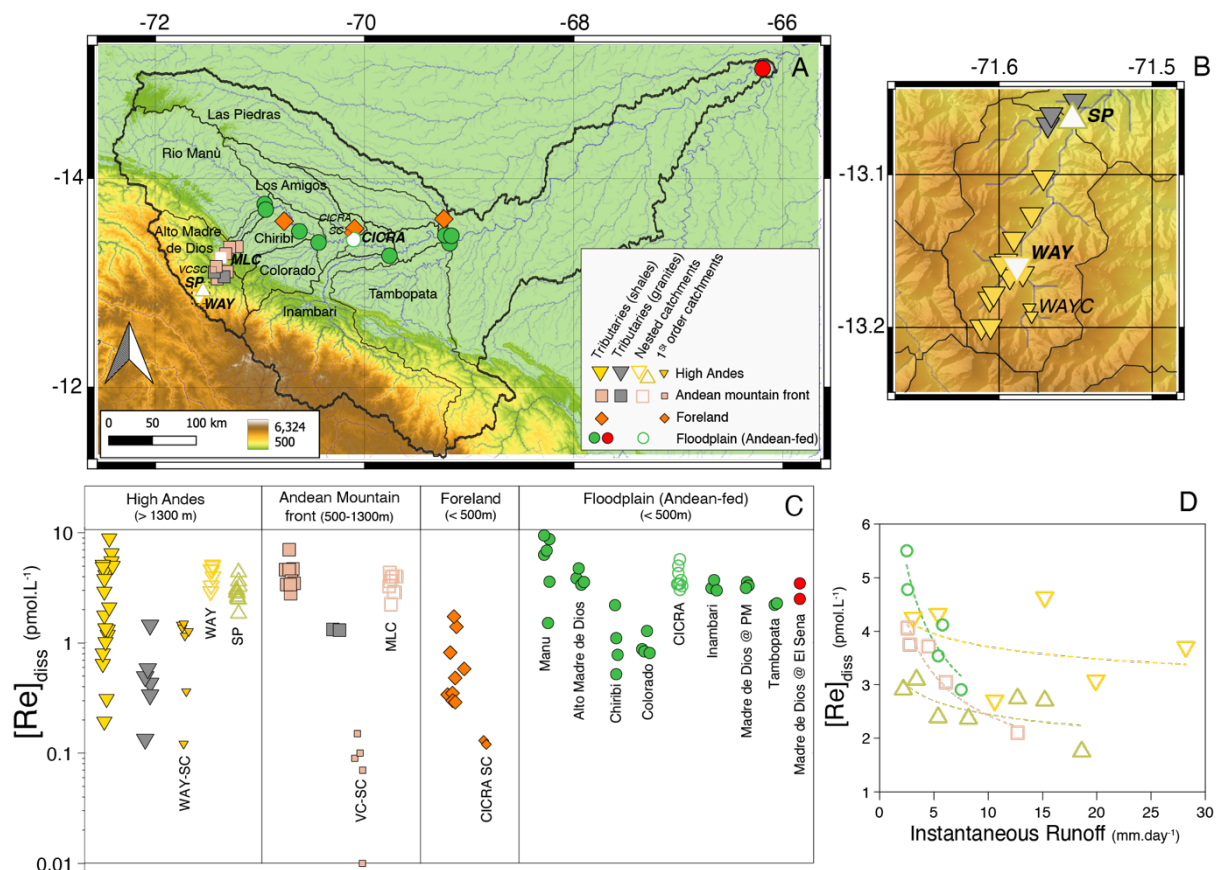
125 To resolve these issues, here we investigate the source, partitioning and fluxes of
126 dissolved and particulate rhenium (Re) in the Madre de Dios watershed, part of the larger
127 Amazon Basin. We focus on an elevation transect ranging from the high Andes to the low-
128 elevation floodplains and use Re to quantify the flux of CO_2 released by OC_{petro} oxidation.
129 These catchments have been well-characterized by previous studies in terms of erosion rates
130 and their major dissolved load (11, 23, 27), and benefit from time-series samples over a range
131 of river discharges. Most importantly, this setting provides an opportunity to determine the rate
132 of OC_{petro} oxidation in each of the different geomorphological settings (mountain, foreland,
133 floodplain) within a single river basin.

134 135 **Study site**

136 The Madre de Dios watershed ($124,231 \text{ km}^2$ at the confluence with the Rio Beni in Bolivia) is
137 one of the main headwaters of the Amazon basin (28), the largest river basin in the world. The
138 precipitation in the Madre de Dios region is between <1000 and $>6000 \text{ mm.yr}^{-1}$ and the mean

139 annual temperature varies with elevation from 4 to 25°C (28–30). The Rio Madre de Dios
140 drains: i) the eastern flank of the Andes in Peru with elevations from 1300 m to 6300 m, ii) the
141 mountain front with elevations from 500 m to 1300 m, iii) the foreland corresponding to
142 elevations of less than 500 m, in which river basins are not Andean-fed but had undergone some
143 recent uplift associated with the Fitzcarrald Arch, and iv) the Andean-fed floodplains, which
144 are the low-relief environments adjacent to active river channels from rivers originating from
145 the Andes and where sediments are deposited and exchanged with the main channel. The
146 bedrock in the headwaters is primarily composed of Paleozoic and Mesozoic sedimentary and
147 metasedimentary rocks and some minor granitic intrusions in the Andes (23).

148 To characterize the spatial variability of dissolved Re concentrations ($[\text{Re}]_{\text{diss}}$) across
149 the Madre de Dios River basin (Fig. 1A), we studied a large number of small tributaries draining
150 each geomorphological setting that have been subject to prior work on water, sediment and
151 carbonate and silicate weathering fluxes (Clark et al., 2017, 2014; Torres et al., 2015, 2017,
152 2016; Burt et al., 2021). To characterize the dissolved Re sources, we sampled stream, spring
153 and lysimeter waters from small first-order catchments in each geomorphological setting
154 (referred as “WAY-SC”, “VC-SC” and “CICRA-SC”; Burt et al., 2022). To examine the
155 downstream evolution of OC_{petro} weathering processes across these geomorphic settings, we
156 studied in detail four main nested sub-catchments that define a geomorphic gradient from the
157 Andes to the Foreland-floodplain: the Rio Kosñipata at Wayqecha in the Andes (referred as
158 “WAY”, altitude 2250 m); the Rio Kosñipata at San Pedro in the Andes (“SP”, altitude 1360
159 m); the Alto Madre de Dios at Manu Learning Center (“MLC”, altitude 479 m) at the transition
160 between the Andes and the Foreland; and the Madre de Dios at CICRA-Los Amigos research
161 station (“CICRA”, altitude 217 m). Time series $[\text{Re}]_{\text{diss}}$ and discharge data from the years 2010-
162 2011 are used to characterize changes in Re concentration during the hydrological cycle. The
163 measured annual runoff for the year 2010-2011 ranged was $3065 \text{ mm}\cdot\text{yr}^{-1}$ at the “WAY” site
164 (Upper Andes) to $2796 \text{ mm}\cdot\text{yr}^{-1}$ at SP. The suspended sediment flux (a proxy for erosion rate)
165 at San Pedro (SP) measured during the same period is $3500 \text{ t}\cdot\text{km}^{-2}\cdot\text{yr}^{-1}$ (11), similar to the
166 estimated suspended sediment load from the Andean area of the Madre de Dios watershed
167 ($3208 \text{ t}\cdot\text{km}^{-2}\cdot\text{yr}^{-1}$; Vauchel et al., 2017). Finally, to integrate weathering processes over large
168 areas and establish a Re mass-budget, we studied several large tributaries with Andean-fed
169 floodplain that drain all geomorphic settings (Rios Manù, Colorado, Chiribi, Inambari and
170 Tambopata).



171
 172 **Fig. 1.** (A) Map of the Madre de Dios River basin with the location of the samples from this study. (B) Inset
 173 showing the location of the samples in the High Andes. (C) Re concentration (in pmol.L⁻¹) in the various
 174 geomorphic settings for all river samples from this study. The [Re]_{diss} from the two hot springs samples are not
 175 shown. (D) [Re]_{diss} versus instantaneous runoff W (water discharge normalized by catchment area, mm day⁻¹) at
 176 the time of sampling for the main nested catchments of this study (WAY, SP, MLC and CICRA).

177 Results

178 Rhenium concentrations were measured on water samples collected from several field
 179 campaigns, including (i) from the Madre de Dios mainstem and major tributaries sampled at
 180 three flow conditions in 2012 and 2013 (23, 32, 35), and again at high and low flow in March
 181 and May 2019 (36), (ii) from time-series samples collected at four nested catchment sites (areas
 182 50 to 27 830 km²) in 2010 and 2011 at various hydrological conditions (Clark et al., 2014;
 183 Torres et al., 2015), and (iii) from another time series of samples collected from smaller first-
 184 order catchments (<1 km² area) across the elevation gradient (33). The time-series dataset is
 185 used to characterize the relationship between Re concentration and instantaneous runoff
 186 (Materials and Methods).

188 Spatial variability of dissolved Re concentrations

189 Rhenium concentrations in dissolved samples (n=133) range from 0.01 to 63 pmol.L⁻¹, with
 190 spatial variability depending on the sample type, bedrock lithology and geomorphic setting
 191 (Fig. 1B; Dataset S1). Rivers have [Re]_{diss} ranging from 0.1 to 9.5 pmol.L⁻¹. The rainwater
 192 sample collected in the Andes has [Re]_{diss} below detection limit ([Re]_{diss} < 0.05 pmol.L⁻¹) while
 193 [Re]_{diss} in the throughfall sample from the same location is 0.36 pmol.L⁻¹. Lysimeter samples
 194 from first-order small catchments in the Andes and in the Foreland have also very low [Re]_{diss},
 195 ranging from 0.09 to 0.12 pmol.L⁻¹ (n=4). In contrast, the two hot springs samples from Aguas
 196 Caliente have very high [Re]_{diss} (39 pmol.L⁻¹ and 63 pmol.L⁻¹). However, the [Re]_{diss} of the Alto

197 Madre de Dios downstream of the hot springs is unchanged compared to $[\text{Re}]_{\text{diss}}$ upstream of
198 the hot springs, suggesting that their contribution to the Re budget is negligible.

199 In terms of lithology, small rivers draining mostly granitic rocks in the High Andes have
200 lower Re concentrations ($0.56 \pm 0.44 \text{ pmol.L}^{-1}$, 1σ , $n=6$) than rivers draining sedimentary rocks
201 ($2.90 \pm 2.06 \text{ pmol.L}^{-1}$, 1σ , $n=25$). Rivers draining the mountain front composed of mostly
202 granites also have lower $[\text{Re}]_{\text{diss}}$ (1.32 pmol.L^{-1} , $n=2$) than those draining sedimentary rocks
203 ($3.88 \pm 1.12 \text{ pmol.L}^{-1}$, 1σ , $n=10$).

204 We observe a notable geomorphic control on $[\text{Re}]_{\text{diss}}$ for the tributaries and first-order
205 catchments draining specific settings, but not for the nested catchments (Fig. 1B). Tributaries
206 draining sedimentary rocks in the High Andes and Mountain front have significantly higher
207 $[\text{Re}]_{\text{diss}}$ ($3.22 \pm 1.82 \text{ pmol.L}^{-1}$, 1σ , $n=38$) than those draining the foreland ($0.70 \pm 0.53 \text{ pmol.L}^{-1}$,
208 1σ , $n=9$). For first-order catchments, $[\text{Re}]_{\text{diss}}$ is the highest in the High Andes (0.12 to 0.48
209 pmol.L^{-1}), as compared to $<0.15 \text{ pmol.L}^{-1}$ in the Mountain front and Foreland. In contrast, no
210 significant change in $[\text{Re}]_{\text{diss}}$ downstream is observed for nested catchments, although the
211 average concentration at WAY ($3.76 \pm 0.76 \text{ pmol.L}^{-1}$, 1σ , $n=6$) is slightly higher than at the SP
212 site ($2.59 \pm 0.44 \text{ pmol.L}^{-1}$, 1σ , $n=7$). We note that in March 2019, $[\text{Re}]_{\text{diss}}$ was higher (4.22
213 pmol.L^{-1}) at SP than the average $[\text{Re}]_{\text{diss}}$ of time-series measurements from the 2010-2011
214 period, perhaps related to a large landslide in this catchment in the intervening period. At the
215 foreland-floodplain site (CICRA), $[\text{Re}]_{\text{diss}} = 3.69 \pm 0.98 \text{ pmol.L}^{-1}$ (1σ , $n=9$). For the main
216 tributaries of the Madre de Dios, we observe the highest $[\text{Re}]_{\text{diss}}$ in the Manù (1.5 to 9.5 pmol.L^{-1})
217 $[\text{Re}]_{\text{diss}}$ in the Chiribi and Colorado rivers (0.5 to 2.2 pmol.L^{-1}), and intermediate
218 $[\text{Re}]_{\text{diss}}$ in the Alto Madre de Dios (3.4 to 4.7 pmol.L^{-1}), Inambari (3.3 pmol.L^{-1}) and the
219 Tambopata (2.3 pmol.L^{-1}).

220

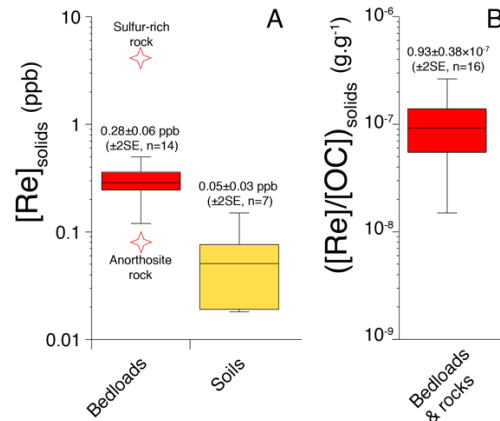
221 **Temporal variability of dissolved Re concentrations**

222 In the four nested-catchments, $[\text{Re}]_{\text{diss}}$ generally decreases with increasing instantaneous runoff,
223 Q , except for the high-altitude Andean site (WAY) where $[\text{Re}]_{\text{diss}}$ shows no clear relationship
224 with runoff (Fig. 1C). The relationship can be modeled using a power law $[\text{Re}]_{\text{diss}} = a \times Q^b$,
225 with a and b as the two fitted constants. For our samples, we observe a decrease of the b value
226 from the Andes (-0.09 ± 0.12 in WAY, -0.15 ± 0.08 in SP; 1σ) to the mountain front (-0.40 ± 0.06
227 in MLC) and the foreland-floodplain (-0.46 ± 0.08 in CICRA), indicating a more chemostatic
228 behavior of Re in the Andes, and more dilutional behavior in the Foreland-floodplain. This
229 decrease of the b value with elevation is similar to that observed for most major elements (27).
230 The correlation coefficient for the power law relationship of rhenium with runoff is the lowest
231 in the Andes ($r^2=0.12$ for WAY and $r^2=0.38$ for SP) and likely reflects the impact that the
232 upstream confluence of tributaries has on geochemical mixing (27, 35).

233

234 **Re concentrations in solids**

235 The Re concentration in bedloads ($[\text{Re}]_{\text{BM}}$) from Andean rivers draining shales ranges from
236 0.12 to 0.50 ppb with an average of $0.28 \pm 0.06 \text{ ppb}$ ($\pm 2\text{SE}$, $n=14$; Fig. 2). These are higher than
237 the Re concentration in Andean soil samples (37) collected close the SP site $0.07 \pm 0.07 \text{ ppb}$
238 ($\pm 2\text{SE}$, $n=3$) and in the Foreland-floodplain $0.04 \pm 0.01 \text{ ppb}$ ($\pm 2\text{SE}$, $n=4$). The $[\text{Re}]_{\text{BM}}$ is slightly
239 higher in WAY (0.31 to 0.36 ppb) compared to SP (0.23 to 0.26 ppb). Two rock samples were
240 analyzed: $[\text{Re}]$ of the OC_{petro} and sulfur-rich sedimentary rock sample is almost 100 times higher
241 (4.61 ppb) than the igneous rock (0.06 ppb). The $[\text{Re}]/[\text{OC}]$ ratio in bedloads and rocks vary
242 from 0.27×10^{-7} to $2.65 \times 10^{-7} \text{ g.g}^{-1}$ with an average of $0.93 \pm 0.38 \times 10^{-7} \text{ g.g}^{-1}$ ($\pm 2\text{SE}$, $n=16$; Fig. 2).
243 The average $[\text{Re}]/[\text{OC}]$ for the Kosñipata stream (WAY and SP sites) is $0.80 \pm 0.12 \times 10^{-7} \text{ g.g}^{-1}$
244 ($\pm 2\text{SE}$, $n=5$). This $[\text{Re}]/[\text{OC}]$ ratio value is similar to bedload from New Zealand Southern Alps
245 (4) but lower than bedloads from Taiwan (17), the Yamuna River (18) and the Mackenzie River
246 (20).



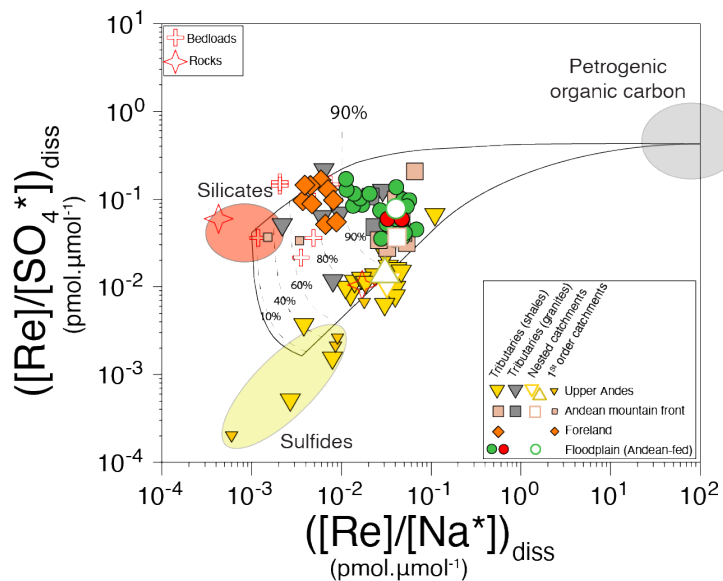
248
 249 **Fig. 2.** (A) Rhenium concentration in solids ($[Re]_{solids}$): rock samples (red stars), bedloads (red box) and
 250 (yellow box). The middle line in boxes is the average value, upper and lower box limits correspond to the $\pm 2SE$
 251 values, the upper and higher bars represent extreme data points. (B) Average $\pm 2SE$ and extreme values of the
 252 $[Re]/[OC]$ ratio in bedloads and rocks.

253 **Discussion**

254 Our aim is to determine the rates and controls of OW of OC_{petro} across the transition from the
 255 Andes Mountains to Amazon floodplain in the Madre de Dios basin. To do so, we need to
 256 characterize the source, behavior, and fluxes of dissolved Re. Following previous studies (4,
 257 17, 19, 20, 38), the OC_{petro} oxidation yield ($J_{OC_{petro-ox}}$, $tC\ km^{-2}\ yr^{-1}$) can be estimated from:

258
 259
$$J_{OC_{petro-ox}} = J_{Re} \times f_c \times ([OC]/[Re]_{petro}) \times (1 - f_{graphite})$$
 [1]
 260

261 Where “ J_{Re} ” is the dissolved Re yield (in $g\ km^{-2}\ yr^{-1}$), the product of the Re concentration
 262 and runoff ($J_{Re} = [Re]_{diss} \times Q$), while “ $([OC]/[Re]_{petro})$ ” is the OC/Re ratio in sedimentary rocks
 263 being weathered (in $g\ g^{-1}$), “ f_c ” is the fraction of dissolved Re deriving from the oxidation of
 264 OC_{petro} and “ $f_{graphite}$ ” is the proportion of graphite in the rocks that may be resilient to chemical
 265 oxidation (14).
 266



267
 268 **Fig. 3.** Rhenium to sodium, $[Re]/[Na^*]$, and rhenium to sulfate, $[Re]/[SO_4^*]$, ratios ($pmol\ \mu mol^{-1}$) for river waters
 269 from this study (High Andes = triangles; Andean Mountain front = square; Foreland = diamond; circles = Foreland-
 270 Floodplains). For the four nested-catchments, only the average values are represented. The red crosses correspond
 271 to the river sediments (bedloads) and bedrocks from the Kosnipata River basin. The shaded ovals show the ranges

272 of elemental ratios associated with the rock weathering end-members (sulfides, silicates and OC_{petro}). The lines
273 correspond to the mixing proportions between the rock weathering end-members, with the average proportion of
274 Re derived from OC_{petro} weathering shown (in %).

275 **Dissolved Re source and yield**

276 To determine the OC_{petro} oxidation flux using the Re proxy, we must first quantify the
277 proportion of dissolved rhenium derived from OC_{petro} oxidation relative to other potential Re
278 sources (rainwater, carbonates, sulfides, silicates, carbonates; Dalai et al., 2002). Following the
279 approach developed in Horan et al., (2019), we use the $[Re]/[SO_4^*]$ and $[Re]/[Na^*]$ ratios to do
280 so ($[Na^*]$ and $[SO_4^*]$ are concentrations corrected for atmospheric-derived contributions). In
281 general sulfides have low Re/ SO_4 (Miller et al., 2011) and silicates low Re/Na relative to OC_{petro}
282 (Horan et al., 2019), and both Na and SO_4 are conservative soluble species in the Madre de
283 Dios catchment (32, 35, 36). In analogy with studies on silicate and carbonate weathering, here
284 we use local constraints on the end member compositions, using the combination of water
285 samples from first-order catchments and tributaries (e.g. Gaillardet et al., 1997; Galy and
286 France-Lanord, 1999), combined with river sediments and rocks (23, 39) (Materials and
287 Methods).

288 We find that small Upper Andes tributaries draining shales have a large range of
289 $[Re]/[SO_4^*]$ and $[Re]/[Na^*]$ ratios that can be interpreted as a mixing trend between sulfides and
290 OC_{petro} weathering, with limited Re contribution from silicate weathering (Fig. 3). In contrast,
291 Andean tributaries draining granites, and rivers draining the foreland, have ratios that can be
292 mostly explained by a mixture between silicates and OC_{petro} (Fig. 3). A mixing analysis
293 (Materials and Methods) shows that the fraction of dissolved Re derived from OC_{petro} oxidation,
294 f_c (Equation 1), is >0.75 in the Andes (sites WAY and SP) and increases downstream to >0.90 .
295 Seasonal variability of the Re source is small but significant (less than 20% variability), with
296 higher proportion of Re derived from OC_{petro} oxidation in the Andes at higher runoff. The
297 fraction of Re derived from sulfide oxidation decreases from ~ 0.15 - 0.25 in the Andes (WAY
298 and SP) to <0.05 in the Foreland-floodplain (CICRA). The fraction of Re derived from silicate
299 weathering is generally <0.05 but reaches ~ 0.2 for rivers draining only the foreland (e.g. Los
300 Amigos River). Altogether, this shows that in the Madre de Dios basin, the majority of
301 dissolved Re is derived from OC_{petro} oxidation, confirming observations in other catchments
302 where sedimentary rocks dominate the geology (19, 20, 40).

303 Calculation of dissolved Re yield (J_{Re}) can be done in several ways, i.e. using average
304 $[Re]_{\text{diss}}$ (4, 17, 18, 41), discharge-weighted average $[Re]_{\text{diss}}$ (42) or rating curve-derived $[Re]_{\text{diss}}$
305 (19) and annual or instantaneous water discharge estimates. Here, these methods return similar
306 results (Materials and Methods; Dataset S3). Therefore, we take advantage of paired $[Re]_{\text{diss}}$
307 and discharge measurements (at the four nested catchment sites and at the main tributaries) and
308 use discharge-weighted average $[Re]_{\text{diss}}$ and annual water discharge to derive dissolved Re
309 yield. For the main tributaries, the highest J_{Re} is in the Manu River catchment ($2.0^{+0.9}/_{-0.7}$ g km⁻²
310 yr⁻¹) and the lowest for the Las Piedras river (0.3 ± 0.1 g km⁻² yr⁻¹). For the nested catchments,
311 the Re yield is 2.1 ± 1.0 g km⁻² yr⁻¹ and 1.3 ± 0.2 g km⁻² yr⁻¹ for WAY and SP sites respectively,
312 and 1.6 ± 0.4 g km⁻² yr⁻¹ for the Foreland-floodplain (CICRA) site. Although there is slight
313 decrease with elevation, the main result is that the specific Re yield of the Rio Alto Madre de
314 Dios does not change, within uncertainty, when the Rio Alto Madre de Dios (Andes) reaches
315 the Foreland-Floodplains.

316

317 **Rates and control of OC_{petro} oxidative weathering in the Andes**

318 We compute the OC_{petro} oxidative weathering rate (Equation 1) using the parameters
319 values defined above (Dataset S3). As we have no constraint on f_{graphite} in this setting and as
320 metamorphic graphite may contain similar proportions of Re as in typical organic rich
321 sediments (43), we do not account for this term here. To estimate the uncertainties, we use

322 Monte Carlo simulations with 10 000 resolutions of the equation with distribution sampling of
323 values within the errors of each parameter (4). The estimated OC_{petro} oxidative weathering
324 values based on dissolved Re yield are $16.7^{+11.9/-8.8} \text{ tC km}^{-2} \text{ yr}^{-1}$ for the WAY site and $11.2^{+4.5/-}$
325 $2.8 \text{ tC km}^{-2} \text{ yr}^{-1}$ for the SP site. The lower uncertainty on the $J_{OC_{\text{petro-ox}}}$ for SP is due to a higher
326 precision on the water flux at this site (31).

327 It has been proposed that physical erosion rate is a major control on the rate of OW
328 (Calmels et al., 2007; Hilton and West, 2020), with a potential role for landslide erosion
329 supplying fresh mineral surfaces (44). The present-day erosion rate of the Rio Kosñipata is
330 high, with values between 1200 and 3500 $\text{t.km}^{-2}.\text{yr}^{-1}$ (11) and frequent landslides (45). The
331 $J_{OC_{\text{petro-ox}}}$ for the Kosñipata and Alto Madre de Dios in the Andes are much higher than in the
332 Mackenzie (0.45 to $1.01 \text{ tC km}^{-2} \text{ yr}^{-1}$) and the Swiss Alps (3.6 to $5.7 \text{ tC km}^{-2} \text{ yr}^{-1}$) characterized
333 by lower erosion rates, and more similar to rivers in New Zealand and Taiwan (4 to 30 tC km^{-2}
334 yr^{-1}) which have higher erosion rates (3). Results from this study thus confirm the general
335 control of erosion rate on the rate of OC_{petro} oxidation. The un-weathered solid OC_{petro} export
336 at the SP site has been determined previously to be $16.1 \pm 1.4 \text{ tC.km}^{-2}.\text{yr}^{-1}$ using sediment
337 samples collected across the same time period (Clark et al., 2017). These fluxes imply that
338 $41 \pm 10\%$ of the total bedrock OC_{petro} is oxidized in the Andes, and the remainder is exported
339 downstream. This OC_{petro} weathering intensity value is slightly lower than in the Mackenzie
340 River basin (50%), similar to the Swiss Alps (19) and higher than in Taiwanese rivers (<20%;
341 Hilton et al., 2014).

342 Our estimate of the flux of OC_{petro} oxidation in the Rio Kosñipata is the first attempt to
343 quantify the CO_2 emission from weathering of OC_{petro} in the Andes. This estimate can also be
344 compared with other carbon fluxes relevant to the long-term carbon cycle in the Andes in the
345 Kosñipata catchment. In the SP catchment, the rate of biospheric organic carbon (OC_{bio}) export
346 in river suspended sediments is $12.6 \pm 0.4 \text{ tC km}^{-2} \text{ yr}^{-1}$ (11), which is comparable and about 13%
347 higher than the OC_{petro} oxidative weathering yield. At the same site, the yield of carbon release
348 associated with carbonate weathering by sulfuric acid is $\sim 6 \text{ tC km}^{-2} \text{ yr}^{-1}$ (23), 45% lower than
349 the rate of CO_2 release by OC_{petro} oxidation. Together, the OW of reduced phases (OC_{petro} and
350 sulfides) in Andean sedimentary rocks release about $17 \text{ tC km}^{-2} \text{ yr}^{-1}$ to the atmosphere,
351 confirming that OW of sedimentary rocks in mountain belt is a large source of CO_2 to the
352 atmosphere.

353

354 **Oxidative weathering in the foreland and in the Andean-fed floodplains**

355 Once the OC_{petro} that survived oxidation in the Andes has reached the foreland and the
356 floodplains, it can undergo further oxidation during transport and deposition in the floodplains
357 (10). It has been suggested that this process can be a large source of CO_2 to the atmosphere in
358 the neighbouring Beni catchment (10) and in the Ganges floodplain (14). Here we take several
359 approaches to isolate the weathering signal from the foreland (here defined as <500 m) versus
360 the Andean-fed floodplain (<500 m and low relief adjacent to active river channels where
361 Andean-derived sediments are exchanged). First, we assess the OC_{petro} weathering flux in the
362 foreland by using data from the Las Piedras river catchment, since it drains the foreland
363 exclusively with no Andean contribution. The $[Re]_{\text{diss}}$ concentration at Las Piedras (1.24 ± 0.35
364 pmol.L^{-1} , 2SE) is low like the two other medium-size foreland rivers, the Blanco (0.36 ± 0.06
365 pmol.L^{-1}) and the Los Amigos ($0.50 \pm 0.16 \text{ pmol.L}^{-1}$). Assuming that the $[Re]/[OC]$ ratio value
366 of bedrock in Las Piedras is similar to the Andes, we calculate a $J_{OC_{\text{petro-ox}}}$ of $1.9^{+1.2/-0.8} \text{ tC.km}^{-2}.$
367 yr^{-1} which is about 6 times lower than in the Andes and similar to the rate measured in the
368 Mackenzie River basin (20).

369 To estimate the OC_{petro} weathering flux in the floodplains, we attempt a mass-balance
370 at the scale of the whole Madre de Dios catchment ($118\,459 \text{ km}^2$). If the $J_{OC_{\text{petro-ox}}}$ from SP
371 (Upper Andes) is representative of the Andean area ($40\,868 \text{ km}^2$; defined as <500 m) of the

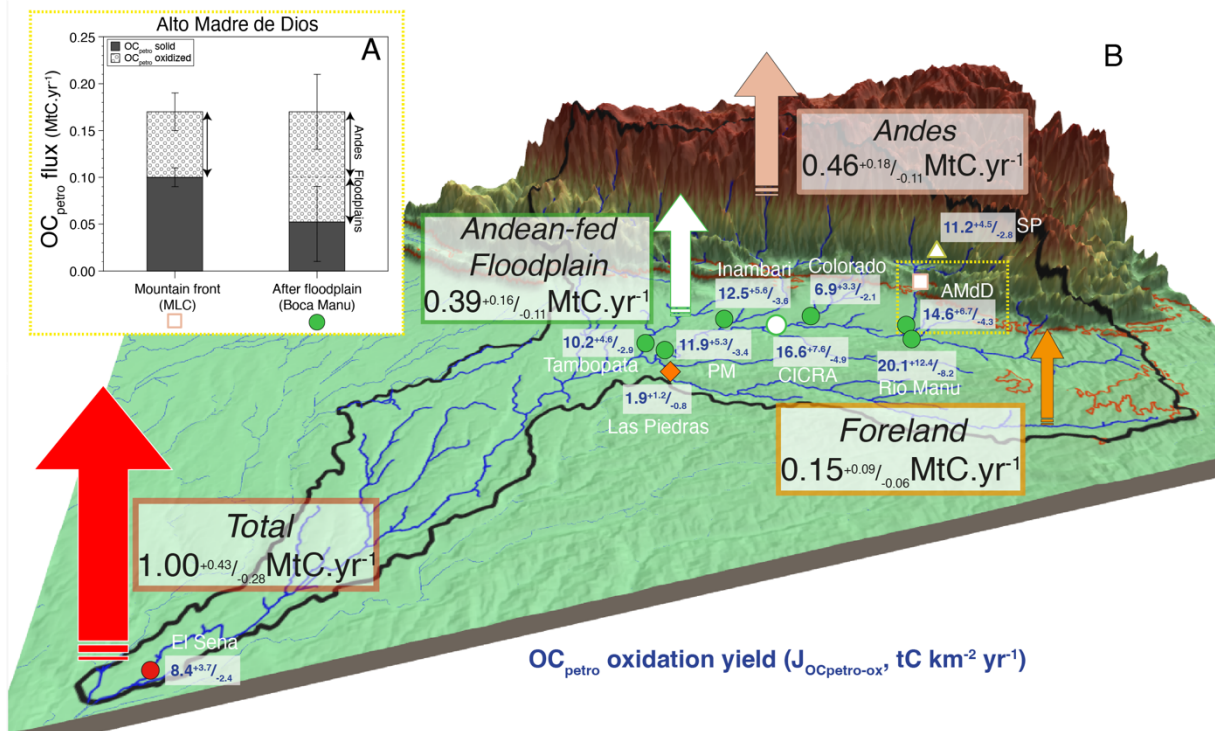
372 Madre de Dios, we calculate a total Andean $J_{OC_{\text{petro-ox}}}$ of $0.46^{+0.18}/_{-0.11}$ MtC.yr⁻¹. This assumption
373 is justified as the SP catchment has similar erosion rates as the inferred Andean erosion rate for
374 the whole Madre de Dios River (34). The contribution from foreland weathering (< 500m; 77
375 591 km²) can be estimated using the $J_{OC_{\text{petro-ox}}}$ from the Las Piedras River (19 630 km²) as
376 $0.15^{+0.09}/_{-0.06}$ MtC.yr⁻¹. The total $J_{OC_{\text{petro-ox}}}$ at the mouth of the Madre de Dios is $1.00^{+0.43}/_{-0.28}$
377 MtC.yr⁻¹. Hence, the contribution of Andes + Foreland is lower than the total $J_{OC_{\text{petro-ox}}}$ of the
378 Madre de Dios at its mouth by $0.39^{+0.16}/_{-0.11}$ MtC.yr⁻¹, which we attribute to weathering in the
379 floodplain. This mass-balance indicates that ~46% of the total OC_{petro} oxidation takes place in
380 the Andes, ~40% in the floodplains, and ~14% in the foreland-lowlands (Fig. 4).

381 The deposition and weathering of sediments in the floodplain constitutes a different
382 mechanism compared to upland weathering (27, 46). Sediment and water exchange during
383 floodplain transit by rivers can influence sediment residence time, water flux, and redox state,
384 which could all facilitate OW (7). In addition, the warmer climatic conditions in the floodplain
385 relative to the Andes could be important in setting rates of reaction rates (21), while the length
386 of floodplains and their channel migration rates (47) could also be important controlling
387 variables. Scaled laboratory experiments have been used to suggest that in-situ oxidation during
388 within river transport is small (48) meaning reactions in sediment stores of floodplains are likely
389 to be of most importance.

390 Our detailed spatial characterization of Re concentrations and fluxes adds constraint on
391 the location of OC_{petro} oxidation reactions in the floodplains. The section of the river along the
392 course of the Alto Madre de Dios floodplain, between the Mountain Front (MLC) and the
393 confluence with the Rio Manu at the Boca Manu Village (Fig. 4A), is mostly braided and multi-
394 channel, with mobile channel bars comprised of sand and fine gravel. Measurements show a
395 significant increase of Re flux. Water isotopes indicate lack of significant water, and therefore
396 likely Re, contribution from tributaries in this river reach (see Materials and Methods). Hence,
397 we attribute this Re flux increase to weathering of OC_{petro} from Andean sediments transiting in
398 the floodplains (Materials and Methods). At Boca Manu, we calculate a $J_{OC_{\text{petro-ox}}}$ rate of
399 $14.6^{+6.7}/_{-4.3}$ tC.km⁻².yr⁻¹ for the Alto Madre de Dios, which is slightly higher than the value in
400 the Andes at SP ($11.2^{+4.5}/_{-2.8}$ tC.km⁻².yr⁻¹). This indicates that the incorporation of the floodplain
401 produces a slight increase of the specific flux of OC_{petro} oxidation. We calculate a total annual
402 $J_{OC_{\text{petro-ox}}}$ flux between MLC (Mountain front) and Boca Manu of 0.05 ± 0.04 MtC.yr⁻¹ (± 1 SD),
403 implying that ~40% of the total CO₂ release through OC_{petro} oxidation in the Alto Madre De
404 Dios catchment upstream Boca Manu takes place in the floodplain, and ~60% in the Andes.
405 This would suggest that ~45% of the solid OC_{petro} load at MLC (0.10 ± 0.01 MtC.yr⁻¹ assuming
406 similar solid OC_{petro} yield as at SP) is oxidized before reaching Boca Manu.

407 In the section between Boca Manu and CICRA, where a larger, single channel meanders
408 through the floodplain, the results are less straightforward (see materials and methods and
409 Dataset S5). We observe a significant contribution from floodplain weathering (20% increase
410 instantaneous Re yield, with an uncertainty of 5%) only during the dry season in 2019. During
411 wet season sampling periods (2013 and 2019), we observe no significant floodplain
412 contribution (within an uncertainty of 10 to 12%). In contrast, for the dry season in 2013, we
413 observe a 16% decrease of Re yield (within an uncertainty of 11%) along the section. Over this
414 transit from MLC to CICRA, the isotopic composition of sulfate suggests minimal sulfate
415 reduction, suggesting that oxygen is available for OW weathering along this river reach. In
416 addition, the warm tropical climate could drive higher reaction rates and OC_{petro} oxidation
417 (Soulet et al., 2021). Therefore, the apparent limited floodplain weathering could reflect an
418 exhaustion of reactive OC_{petro} supplied from Andean erosion upstream. Regardless of the
419 mechanisms at play, the Rio Madre de Dios example shows that high rates of OC_{petro} oxidation
420 in the mountain headwaters can be matched by OW in the foreland (Fig. 4). A large proportion

421 of floodplain weathering appears to happen over a relatively short-length scale ($\sim <85$ km) after
 422 exiting the Andes.



423
 424
 425 **Fig. 4.** (A) Annual river flux of solid OC_{petro} (black) and oxidized OC_{petro} (light grey and white) from the Alto
 426 Madre de Dios sub-catchment. (B) Estimated net contribution (vertical arrows) of each geomorphic zones to the
 427 total flux of OC_{petro} oxidation and associated CO₂ release at the scale of the whole Madre de Dios River basin.
 428 Main tributaries annual river yield (in blue) of OC_{petro} oxidation derived from Re measurements are also indicated.
 429 SP=San Pedro, AMdD=Alto Madre de Dios at Boca Manu, PM=Madre de Dios at Puerto Maldonado, El
 430 Sena=Madre de Dios at El Sena. The red squiggly line corresponds to the 500m elevation.

431
 432 **Implications for the long-term carbon cycle**

433 Previous study on the Amazon River found significant CO₂ release from OC_{petro}
 434 oxidation during the transit of fluvial sediments in the Madeira floodplain (10, 11). They found
 435 that the solid OC_{petro} flux from the Madeira at the confluence with the Amazon is much lower
 436 than the solid OC_{petro} supplied by the Beni at the mountain front and transported through the
 437 plain. They estimated a CO₂ emission of 0.50 MtC.yr⁻¹ across the Rio Beni floodplain. Our Re-
 438 based estimate of OC_{petro} oxidation during the transit of Madre de Dios sediments in the
 439 floodplain (0.39^{+0.16}/_{-0.11} MtC.yr⁻¹) is of similar magnitude. Combined, this release of CO₂ is
 440 approximately double the silicate weathering CO₂ drawdown of the whole Madeira river basin
 441 (49). The total CO₂ emission from OC_{petro} oxidation in the whole Madre de Dios catchment
 442 (1.00^{+0.43}/_{-0.28} MtC.yr⁻¹) is also more than twice the silicate weathering CO₂ drawdown
 443 (0.43^{+0.22}/_{-0.09} MtC.yr⁻¹; Moquet et al., 2011). Considering that sulfide oxidation also contributes
 444 to the carbonate weathering flux (Torres et al., 2016), the net CO₂ balance during weathering
 445 in the Madre de Dios catchment appears to be tipped firmly toward being a CO₂ source (Hilton
 446 and West, 2020).

447 Our findings from the Rio Madre de Dios catchment allow us to postulate a broader role
 448 for floodplain weathering in enhancing the CO₂ release by OC_{petro} oxidation. Uplift and
 449 exhumation of sedimentary rocks in a mountain range can increase the supply of OC_{petro} to an
 450 oxygenated weathering zone (Soulet et al., 2021; Hilton et al., 2014) and increase the rates of
 451 OC_{petro} oxidation and CO₂ release, as we observe in the Andes (Fig. 4). However, the overall
 452 weathering intensity can be low, with only $\sim 20\%$ to 50% of OC_{petro} oxidized, meaning there is

453 further potential for CO₂ release. On high standing mountain islands, floodplains are short and
454 un-weathered OC_{petro} could be re-buried offshore, as is the case for the Taiwan orogen (Sparkes
455 et al., 2020). However, if the tectonic setting permits the growth of a continental floodplain,
456 additional OC_{petro} oxidation is very likely to occur (Fig. 4), potentially until only extremely
457 refractory OC_{petro} escapes oxidation (Bouchez et al., 2010). While future work will need to
458 establish how temperature and O₂-supply impact OC_{petro} oxidation rates in floodplains (Bolton
459 et al., 2006; Soulet et al., 2021), our results suggest that the formation of floodplain adjacent to
460 a mountain range allows more complete OC_{petro} oxidation during sediment transit, and the
461 growth and waning of riverine floodplains could act as a powerful carbon cycle modifier
462 throughout Earth's history.

463

464 **Materials and methods**

465 The materials and methods are summarized here; further details are provided in SI Appendix. All data
466 used in this study are reported in Datasets S1–S5.

467

468 **Sample collection and discharge measurements.** Major cation and anion concentration data of
469 samples from 2010 to 2013 are from Torres et al., (2015, 2016). Detailed information on the sampling
470 protocol can be found in those studies. In summary here, for the four main nested catchment sites (WAY,
471 SP, MLC and CICRA, Fig. 1), time-series samples were collected between 2010 and 2011 using a clean
472 PP bottle and filtered on site with 0.2 μm porosity nylon filter (27). At these sites, water discharge was
473 measured at the same time as sampling by monitoring water levels manually and converting to discharge
474 using a rating curve. At the SP site, river level was monitored with a water level logger that recorded
475 river level measurements every 15 min (31). At other localities, samples were collected on fieldtrips in
476 2012, 2013, 2016 and 2019 (Dataset S1). Water samples were collected from the river surface using
477 clean bucket and transferred to 10 or 20 L plastic bags before filtration. Samples were filtered within 24
478 to 48h of collection with 0.2μm porosity polyethersulfone (PES) filters. The discharge (“Q”) at CICRA
479 was measured during each sampling trip using an Acoustic Doppler Current Profiler (ADCP, RD1
480 Sentinel GED154 in March 2013 and SonTek M9 in August 2013 and in March and May 2019). In
481 2019, the discharge of the Alto Madre de Dios, Rio Manù, Chiribi and Colorado were also measured by
482 ADCP. All discharge measurements are from Torres et al., (2017) and Burt et al., (2021)

483

484 **Re concentration measurements in water and sediments.** The dissolved Re concentrations were
485 measured following the same protocol as described in Hilton et al., (2021). Briefly, dissolved Re
486 concentrations ([Re]_{diss}) were measured by direct calibration against a set of seven standards with
487 varying Re abundances and similar matrixes to river water, by quadrupole inductively coupled plasma
488 mass spectrometry (Q-ICP-MS, Agilent Technologies 7900). Calibration standards and samples were
489 doped with 0.025 mg/L concentration of internal standard Tb and Bi to correct for instrumental drift and
490 matrix drift. Accuracy and precision of the measurements was assessed by repeated measurements of
491 various riverine standard reference materials, in particular reference materials SLRS-5 and SLRS-6 at
492 various dilutions. The standards confirmed better than 10% accuracy and precision. For sediment
493 samples, the rhenium concentrations were determined using the method in Dellinger et al., (2020). A
494 mass of 0.2 to 0.5g was digested using a mixture of 3 mL 27M HF and 3 mL 16M HNO₃ for 24 to 48h
495 at 120°C on a hot plate. Digested solutions were processed through AG1-X8 resin to separate Re from
496 the rest of the matrix. Rhenium concentrations were then measured with a Neptune MC ICP-MS at
497 Durham University.

498

499 **Dissolved Re yield calculations.** Several methods can be used to determine dissolved ion yields
500 depending on the number of paired water discharge (Q) and concentration measurements, their
501 frequency and the behavior of the element of interest in relation with discharge (51). Previous studies
502 with large datasets of Re concentration and discharge (Horan et al., 2019; Hilton et al., 2021) have used
503 a rating curve approach to quantify dissolved yields, by fitting power law functions to the trends in the
504 data and using this relationship to predict predicted for each daily discharge value and annual fluxes.

505 Other studies have used discharge-weighted average concentration (42) or average concentration of
506 several measurements (4, 17, 18, 41) combined with annual water discharge estimates.

507 The four nested catchments in our dataset have between five and nine Q and $[\text{Re}]_{\text{diss}}$ data pairs
508 for each catchment (Fig. 1C). For the large tributaries (Manu, Colorado, Chiribi, Alto Madre de Dios),
509 our dataset includes 4 paired Q and $[\text{Re}]_{\text{diss}}$ measurements each. For all the sites, we use three different
510 methods to calculate the Re yield and uncertainties: i) mean $[\text{Re}]_{\text{diss}} \pm \text{SE}$ multiplied by annual discharge;
511 ii) discharge-weighted mean $[\text{Re}]_{\text{diss}} \pm \text{SE}$ multiplied by annual discharge; and iii) average of measured
512 instantaneous Re fluxes, $J_{\text{Re}} \pm \text{SE}$. The advantage of the first method is that it includes more $[\text{Re}]_{\text{diss}}$
513 measurements (since the instantaneous discharge was not measured for all samples). The disadvantage
514 is that there is a potential bias toward high concentration by not weighting to discharge. The third method
515 is useful if annual discharge is not known, however it has the disadvantage of being less accurate because
516 instantaneous fluxes vary more than instantaneous concentrations (51). Discharge values and
517 uncertainties are reported in Dataset (S3). For the WAY and SP catchments, we use annual discharge
518 values from Clark et al., (2014), determined over the year 2010. In addition, we use average annual
519 discharge values dataset for the main tributaries of the Madre de Dios that were determined by water
520 balance over the period 1968-1982 (52). They calculate a total discharge at the mouth of the Madre de
521 Dios (Riberalta) of $6369 \text{ m}^3 \cdot \text{s}^{-1}$ which are very close (only 12% higher) to the discharge measured during
522 the 2002–2011 period ($5661 \text{ m}^3 \cdot \text{s}^{-1}$; Vauchel et al., 2017). For CICRA, the discharge can be estimated
523 by adding the annual discharge values of the Manu, Alto Madre de Dios, Colorado from Abastos Lara,
524 (1987) and considering that the Rio Chiribi contributes 7.5% of the total discharge in CICRA (see
525 Dataset S5). This gives a value of $2165 \text{ m}^3 \cdot \text{s}^{-1}$. For instantaneous discharge of the main tributaries (Alto
526 Madre de Dios, Manu, Chiribi and Colorado) that were measured or calculated during the 2013 and
527 2019 sampling trip, we use values from Torres et al., (2017) and Burt et al., (2021).

528 Calculation of uncertainty is done by a Monte Carlo simulation (run 10 000 times for each
529 watershed). As the calculated distributions follow skewed rather than normal distributions, we report
530 the median value (50th percentile) with the uncertainty range defined by the 16th and 84th percentiles
531 (equivalent to 68% of the entire population; SI Appendix). Comparison between the various methods
532 shows good agreement between the different methods for the different sites within uncertainties (Dataset
533 S3). The third method gives larger uncertainty compared to methods 1 and 2. This could reflect the
534 lower number of samples used, the uncertainty on the discharge measurement or an imbalance between
535 the discharge during the 1968-1982 period and the 2010-2020 period. When quantifying OC_{petro}
536 oxidation fluxes from the dissolved Re flux for all sites, we use the second method (discharge-weighted
537 $[\text{Re}]_{\text{diss}}$) when possible and the first method (mean $[\text{Re}]_{\text{diss}}$) otherwise.

538
539 **Source partitioning of dissolved rhenium.** To quantify the OC_{petro} oxidation flux using dissolved Re,
540 we need to: i) correct for Re inputs from precipitation and/or atmospheric deposition; ii) quantify the Re
541 input from non- OC_{petro} sources (i.e. sulfide, carbonate and silicate minerals). Solutes in precipitation can
542 come from dissolution of sea salts, dust or biogenic particles. The $[\text{Re}]/[\text{Cl}]$ ratio ($\sim 7.5 \times 10^{-5} \text{ pmol} \cdot \mu\text{mol}^{-1}$)
543 of the ocean is very low (53) compared to the $[\text{Re}]/[\text{Cl}]$ of rivers from the Madre de Dios. The $[\text{Cl}]_{\text{diss}}$
544 in rivers from this study are also low, indicating that the proportion of Re derived from sea salts is very
545 small. While we have only one rainwater sample from the upper Andes, its $[\text{Re}]_{\text{diss}}$ was below detection
546 limit of the measurement session ($< 0.05 \text{ pmol} \cdot \text{L}^{-1}$), supporting this conclusion. Among all the samples,
547 the lowest measured $[\text{Re}]_{\text{diss}}$ and $[\text{Re}]/[\text{Cl}]$ ratio correspond to a lysimeter sample in the Foreland
548 (PER19-38) with values of $0.009 \text{ pmol} \cdot \text{L}^{-1}$ and $1.4 \times 10^{-3} \text{ pmol} \cdot \mu\text{mol}^{-1}$ respectively. The $[\text{Re}]/[\text{Cl}]$ ratio
549 of this sample is ~ 20 times higher than the $[\text{Re}]/[\text{Cl}]$ ratio of the ocean. The major element concentration
550 for this sample is in the range of the average composition of rainwater from the Andes from Torres et
551 al., (2015). Hence, we use this sample as representative of the maximum Re/Cl ratio of rainwater. For
552 calculating the proportion of Re derived from each source we used the following mass-balance. For the
553 contribution of the rain:

$$555 \quad [\text{Re}]_{\text{rain}} = \left(\frac{\text{Re}}{\text{Cl}} \right)_{\text{rain}} \times [\text{Cl}]_{\text{cycl}} \quad [1]$$

556
557 Where $(\text{Re}/\text{Cl})_{\text{rain}}$ is the proposed elemental ratio between Re and the Cl in the rain ($1.4 \times 10^{-3} \text{ pmol} \cdot \mu\text{mol}^{-1}$)
558 and $[\text{Cl}]_{\text{cycl}}$ is the cyclic chlorine concentration. Since the marine evaporite contribution is small or

559 negligible in the Madre de Dios catchment (23, 27), we consider that $[Cl]_{cycl} = [Cl]_{riv}$. The concentration
 560 of any element X corrected for rainwater and evaporite inputs is referred as “[X*]”. We find that the
 561 proportion of riverine Re deriving from rainfall is negligible, being generally less than 0.5%, with a
 562 maximum of 6%. For SO₄ rain concentration we use a (SO₄/Cl) value of 0.53 corresponding to the
 563 median value of precipitation data from Torres et al., (2015). This value is only slightly lower than the
 564 lowest (SO₄/Cl) measured in our dataset (sample PER19-38, value of 0.60).

565 We then move to quantify the proportion of dissolved rhenium derived from OC_{petro} oxidation
 566 relative to other potential Re sources (sulfides, silicates, carbonates). Previous work has suggested
 567 carbonates are not a major source of dissolved Re (18). If the Re/Ca of carbonates is $\sim 5 \times 10^{-5}$ pmol.mol⁻¹
 568 (18), <1% of total dissolved Re in the studied rivers here can be accounted for by carbonate weathering
 569 (a maximum proportion using this Re/Ca ratio and assuming all dissolved Ca in the Madre de Dios
 570 catchments is derived from carbonates). We therefore follow the approach developed in Horan et al.,
 571 (2019), that uses the (Re/SO₄)* and (Re/Na)* ratio to characterized Re input from sulfides, silicates and
 572 OC_{petro}.

573 Sulfides have low Re/S (Miller et al., 2011) and silicates low Re/Na relative to OC_{petro} (Horan
 574 et al., 2019) and both Na and SO₄ are conservative soluble species in the Madre de Dios catchment
 575 (Baronas et al., 2017; Torres et al., 2017; Burt et al., 2021). Assuming that all the [SO₄²⁻*] is derived
 576 from pyrite oxidation (i.e. no evaporite contribution, Torres et al., 2016), we estimate the Re
 577 concentration derived from sulfide oxidation:

$$579 \quad [Re]_{diss.sulfides} = \left(\frac{Re}{SO_4^{2-}} \right)_{sulfides} \times [SO_4^{2-} *] \quad [2]$$

580
 581 Where (Re/SO₄²⁻)_{sulfides} is the sulfide composition. Then we can determine the concentration of
 582 Re deriving from silicate weathering ([Re]_{diss.sil}) using sodium and assuming that all the [Na*] is derived
 583 from silicate weathering:

$$585 \quad [Re]_{diss.sil} = \left(\frac{Re}{Na} \right)_{silicates} \times [Na *] \quad [3]$$

586
 587 Where (Re/Na)_{sil} is the silicate signature. Then we attribute the excess Re to the oxidation of
 588 OC_{petro}, calculated as:

$$590 \quad [Re]_{diss.OC} = [Re *] - [Re]_{diss.sulfides} - [Re]_{diss.sil} \quad [4]$$

592 In analogy with studies on silicate and carbonate weathering, we use small tributaries (e.g.
 593 Gaillardet et al., 1997; Galy and France-Lanord, 1999) and/or sediment composition (23, 39) to
 594 constrain local weathering end-members [Re]/[SO₄] and [Re]/[Na] ratio values (20). Small Andean
 595 tributaries draining sulfur-rich metasedimentary rocks display two orders of magnitude variability in
 596 [Re]/[SO₄*] and [Re]/[Na*] ratios and are positively correlated. Several Andean rivers with low
 597 [Re]/[SO₄*] values (Fig. 3) have similar composition to the median Re/S values of pyrite from the
 598 literature ($1.8^{+4.2/-1.7} \times 10^{-3}$ pmol.μmol⁻¹, Miller et al., 2011) with the lowest [Re]/[SO₄²⁻]
 599 corresponding to a lysimeter sample (PER19-97) in the riparian area of a small catchment ([Re]*/[SO₄²⁻]
 600]* = 2.2×10^{-4} pmol.μmol⁻¹) and a river sample (r2400) from another small catchment in the Andes
 601 ([Re]*/[SO₄²⁻]* = 4.8×10^{-4} pmol.μmol⁻¹). They both have high SO₄ concentration indicating a high rate
 602 of sulfide oxidation. The [Re]/[SO₄*] ratio of these samples is similar to the sulfide-oxidation rich
 603 sample in the Mackenzie basin (Horan et al., 2019). Hence, this suggests that the Re and SO₄
 604 composition of these rivers is dominated by sulfide oxidation of pyrite and that they can be used as end-
 605 member value for (Re/SO₄)_{sulfides}. The lowest (Re/SO₄)* value (2.2×10^{-4} pmol.μmol⁻¹) measured here
 606 could represent the most “pure” sulfide oxidation end-member and higher [Re]/[SO₄*] for other rivers
 607 would be explained by a small contribution of Re from rock organic carbon oxidation. Alternatively, it
 608 is possible that the Re/S from the local bedrock is variable and explains the range of [Re]/[SO₄*]
 609 observed in rivers dominated by sulfide oxidation. A third possibility is that the very low [Re]/[SO₄*]
 610 and [Re]/[Na*] of some samples is due to non-conservative behavior and removal of dissolved Re
 611 because some of these rivers have low pH values (as low as 3.5) and ReO₄⁻ is less stable under acidic

612 conditions (55). However, this cannot explain the low $[\text{Re}]/[\text{SO}_4^*]$ value of sample PER19-3 (3.5×10^{-3}
613 $\text{pmol} \cdot \mu\text{mol}^{-1}$) which has pH value of 8. Considering the above discussion we consider $(\text{Re}/\text{SO}_4)_{\text{sulfides}}$
614 ranging from 2×10^{-4} to 4×10^{-3} $\text{pmol} \cdot \mu\text{mol}^{-1}$ that encompass the range of $[\text{Re}]/[\text{SO}_4^*]$ of Andean rivers
615 that we identified as typical of sulfide oxidation.

616 Rivers draining mostly granites (sulfide-poor and no OC_{petro}) have low Re/Na but an order of
617 magnitude higher $[\text{Re}]/[\text{SO}_4]$ ratios relative Andean tributaries draining shales (Fig. 3). Interestingly,
618 rivers and lysimeter samples from the foreland have similar composition as rivers draining granites. For
619 Foreland rivers, especially at low elevations, deeply weathered soils and high weathering intensity
620 probably leads to almost complete oxidation of pyrite due to its fast kinetics, and therefore we expect
621 the chemical composition of those samples to be less influenced by OW of pyrite than Andean rivers.
622 Altogether, rivers draining granite and the foreland have ratios that are inferred to reflect mostly mixing
623 between weathering of silicates and weathering of OC_{rock} . These observations are supported by river bed
624 sediment samples. For Andean rivers, the $[\text{Re}]/[\text{Na}]$ ratio of river bed sediments is similar to the low
625 $[\text{Re}]/[\text{Na}]$ of small tributaries draining granites (lowest value is 2.2×10^{-3} $\text{pmol} \cdot \mu\text{mol}^{-1}$ for sample
626 PER19-26) and of samples from small first-order catchments draining the foreland (lowest value is
627 1.5×10^{-3} $\text{pmol} \cdot \mu\text{mol}^{-1}$ for sample PER19-35). In addition, one rock sample, corresponding to an igneous
628 rock (a granophyre), has a very low $[\text{Re}]/[\text{Na}]$ ratio of 4.3×10^{-4} $\text{pmol} \cdot \mu\text{mol}^{-1}$, similar to the crystalline
629 rock endmember $[\text{Re}]/[\text{Na}]$ ratio value in the Himalaya (2×10^{-4} $\text{pmol} \cdot \mu\text{mol}^{-1}$, Ref 18). Hence, we
630 consider here a $[\text{Re}]/[\text{Na}]$ ratio between 4×10^{-4} and 2×10^{-3} $\text{pmol} \cdot \mu\text{mol}^{-1}$ for silicates, which spans the
631 range of lowest $[\text{Re}]/[\text{Na}]$ values from local solid and river samples.

632 Using Eq. (1-4) and the range of above defined $(\text{Re}/\text{SO}_4)_{\text{sulfides}}$ and $(\text{Re}/\text{Na})_{\text{silicates}}$ values for our
633 study area, we can calculate $[\text{Re}]_{\text{diss.OC}}$ for each sample. The calculation of $[\text{Re}]_{\text{diss.OC}}$ is done by a Monte
634 Carlo simulation (run 10 000 times for each river) assuming random distribution of $(\text{Re}/\text{SO}_4)_{\text{sulfides}}$ values
635 between 2×10^{-4} and 4×10^{-3} $\text{pmol} \cdot \mu\text{mol}^{-1}$ and $(\text{Re}/\text{Na})_{\text{silicates}}$ values between 4×10^{-4} and 2×10^{-3} $\text{pmol} \cdot \mu\text{mol}^{-1}$
636 (SI Appendix; Dataset S4). Fractions of dissolved Re derived from OC_{petro} OW ($f_c = [\text{Re}]_{\text{diss.OC}}/[\text{Re}]_{\text{diss}}$)
637 are reported in Dataset S3.

638
639 **Floodplain mass-balance of dissolved Re.** The section of the Alto Madre de Dios river between MLC
640 (mountain front) and Boca Manu (confluence with Manu River) has relatively minimal tributary input.
641 Over three sampling trips, we observe an increase in the Re concentration between MLC and Boca Manu
642 by 3% (March 2013), 26% (March 2019) and 12% (May 2019). There is also a systematic increase in
643 Re/Na and Re/SO₄ ratio. The Re concentration of sub-Andean tributaries is about 0.8 ppt, which is
644 higher than the Re concentration at MLC and could explain part of the observed increase. The
645 contribution of water and weathering inputs from sub-Andean-foreland tributaries can be assessed using
646 δD and $\delta^{18}\text{O}$ since tributaries (PER19-53, Rio Carbon, Rio Pini Pini) have higher δD (-54.9 to -70.2‰)
647 and $\delta^{18}\text{O}$ values (-8.2 to -10.4 ‰) compared to the Alto Madre de Dios at MLC ($\delta\text{D} \sim -72.5\%$ and $\delta^{18}\text{O}$
648 $\sim -10.6\%$). The δD and $\delta^{18}\text{O}$ of the Alto Madre de Dios does not change significantly which indicates
649 that any Re contribution from these tributaries is too small to explain the observed 25% increase in Re
650 concentration in 2019. Therefore, we conclude that this increase is due to ongoing OC_{petro} oxidation of
651 sediment during transit and/or within the floodplain between MLC and Boca Manu.

652

653 Acknowledgments

654 This research was funded by an ERC Starting Grant – ROC-CO2 (678779) to R. G. Hilton, by
655 a European Union COFUND/Durham Junior Research Fellowship (267209) to M. Dellinger
656 and by a National Science Foundation award EAR-1455352 to A.J. West. We thank Amazon
657 Journeys Nature Lodges and Amazon Conservation Association (Peru) for field support. We
658 thank Martin West for laboratory support in Durham and we thank Julien Bouchez for providing
659 the two Madre de dios samples collected near the El Sena station. We thank William Santini
660 for discussions on existing discharge data. We thank Kim Genuite for his help in designing the
661 figure 4.

662

663 References

664 1. R. A. Berner, A. C. Lasaga, R. M. Garrels, The carbonate-silicate geochemical cycle and its effect

- 665 on atmospheric carbon dioxide over the past 100 million years. *Am. J. Sci* **283**, 641–683 (1983).
- 666 2. M. E. Raymo, W. F. Ruddiman, P. N. Froelich, Influence of late Cenozoic mountain building on
667 ocean geochemical cycles. *Geology* **16**, 649–653 (1988).
- 668 3. R. G. Hilton, A. J. West, Mountains, erosion and the carbon cycle. *Nature Reviews Earth &*
669 *Environment* **1**, 284–299 (2020).
- 670 4. K. Horan, *et al.*, Mountain glaciation drives rapid oxidation of rock-bound organic carbon. *Science*
671 *Advances* **3**, e1701107 (2017).
- 672 5. M. A. Torres, A. J. West, G. Li, Sulphide oxidation and carbonate dissolution as a source of CO₂
673 over geological timescales. *Nature* **507**, 346–349 (2014).
- 674 6. R. A. Berner, Biogeochemical cycles of carbon and sulfur and their effect on atmospheric oxygen
675 over phanerozoic time. *Global and Planetary Change* **1**, 97–122 (1989).
- 676 7. E. W. Bolton, R. A. Berner, S. T. Petsch, The Weathering of Sedimentary Organic Matter as a
677 Control on Atmospheric O₂: II. Theoretical Modeling. *Am J Sci* **306**, 575–615 (2006).
- 678 8. D. Calmels, J. Gaillardet, A. Brenot, C. France-Lanord, Sustained sulfide oxidation by physical
679 erosion processes in the Mackenzie River basin: Climatic perspectives. *Geology* **35**, 1003–1006
680 (2007).
- 681 9. J. Spence, K. Telmer, The role of sulfur in chemical weathering and atmospheric CO₂ fluxes:
682 Evidence from major ions, $\delta^{13}\text{CDIC}$, and $\delta^{34}\text{SSO}_4$ in rivers of the Canadian Cordillera.
683 *Geochimica et Cosmochimica Acta* **69**, 5441–5458 (2005).
- 684 10. J. Bouchez, *et al.*, Oxidation of petrogenic organic carbon in the Amazon floodplain as a source
685 of atmospheric CO₂. *Geology* **38**, 255–258 (2010).
- 686 11. K. E. Clark, *et al.*, Erosion of organic carbon from the Andes and its effects on ecosystem carbon
687 dioxide balance. *Journal of Geophysical Research: Biogeosciences* **122**, 449–469 (2017).
- 688 12. Y. Copard, P. Amiotte-Suchet, C. Di-Giovanni, Storage and release of fossil organic carbon
689 related to weathering of sedimentary rocks. *Earth and Planetary Science Letters* **258**, 345–357
690 (2007).
- 691 13. V. Galy, B. Peucker-Ehrenbrink, T. Eglinton, Global carbon export from the terrestrial biosphere
692 controlled by erosion. *Nature* **521**, 204–207 (2015).
- 693 14. V. Galy, O. Beyssac, C. France-Lanord, T. Eglinton, Recycling of Graphite During Himalayan
694 Erosion: A Geological Stabilization of Carbon in the Crust. *Science* **322**, 943–945 (2008).
- 695 15. E. L. Leithold, N. E. Blair, D. W. Perkey, Geomorphologic controls on the age of particulate
696 organic carbon from small mountainous and upland rivers. *Global Biogeochemical Cycles* **20**
697 (2006).
- 698 16. R. B. Sparkes, N. Hovius, A. Galy, J. T. Liu, Survival of graphitized petrogenic organic carbon
699 through multiple erosional cycles. *Earth and Planetary Science Letters* **531**, 115992 (2020).
- 700 17. R. G. Hilton, J. Gaillardet, D. Calmels, J.-L. Birck, Geological respiration of a mountain belt
701 revealed by the trace element rhenium. *Earth and Planetary Science Letters* **403**, 27–36 (2014).
- 702 18. T. K. Dalai, S. K. Singh, J. R. Trivedi, S. Krishnaswami, Dissolved rhenium in the Yamuna river
703 system and the Ganga in the Himalaya: role of black shale weathering on the budgets of Re, Os,
704 and U in rivers and CO₂ in the atmosphere. *Geochimica et Cosmochimica Acta* **66**, 29–43 (2002).
- 705 19. R. G. Hilton, *et al.*, Concentration-Discharge Relationships of Dissolved Rhenium in Alpine
706 Catchments Reveal Its Use as a Tracer of Oxidative Weathering. *Water Resources Research* **57**,
707 e2021WR029844 (2021).
- 708 20. K. Horan, *et al.*, Carbon dioxide emissions by rock organic carbon oxidation and the net
709 geochemical carbon budget of the Mackenzie River Basin. *Am J Sci* **319**, 473–499 (2019).
- 710 21. G. Soulet, *et al.*, Temperature control on CO₂ emissions from the weathering of sedimentary rocks.
711 *Nat. Geosci.*, 1–7 (2021).
- 712 22. T. M. Blattmann, *et al.*, Sulphuric acid-mediated weathering on Taiwan buffers geological
713 atmospheric carbon sinks. *Scientific Reports* **9**, 2945 (2019).
- 714 23. M. A. Torres, *et al.*, The acid and alkalinity budgets of weathering in the Andes–Amazon system:
715 Insights into the erosional control of global biogeochemical cycles. *Earth and Planetary Science*
716 *Letters* **450**, 381–391 (2016).
- 717 24. J. D. Hemingway, *et al.*, Microbial oxidation of lithospheric organic carbon in rapidly eroding
718 tropical mountain soils. *Science* **360**, 209–212 (2018).
- 719 25. R. G. Hilton, A. Galy, N. Hovius, M.-J. Horng, H. Chen, Efficient transport of fossil organic

- 720 carbon to the ocean by steep mountain rivers: An orogenic carbon sequestration mechanism.
721 *Geology* **39**, 71–74 (2011).
- 722 26. Z. Yu, C. Colin, F. Bassinot, S. Wan, G. Bayon, Climate-Driven Weathering Shifts Between
723 Highlands and Floodplains. *Geochemistry, Geophysics, Geosystems* **21**, e2020GC008936 (2020).
- 724 27. M. Torres, A. Joshua West, K. E. Clark, Geomorphic regime modulates hydrologic control of
725 chemical weathering in the Andes-Amazon. *Geochimica et Cosmochimica Acta* (2015)
726 <https://doi.org/10.1016/j.gca.2015.06.007> (July 4, 2015).
- 727 28. M. Thieme, *et al.*, Freshwater conservation planning in data-poor areas: An example from a remote
728 Amazon basin (Madre de Dios River, Peru and Bolivia). *Biological Conservation* **135**, 484–501
729 (2007).
- 730 29. J. C. Espinoza, *et al.*, Rainfall hotspots over the southern tropical Andes: Spatial distribution,
731 rainfall intensity, and relations with large-scale atmospheric circulation. *Water Resources*
732 *Research* **51**, 3459–3475 (2015).
- 733 30. J. Rapp, M. Silman, Diurnal, seasonal, and altitudinal trends in microclimate across a tropical
734 montane cloud forest. *Climate Research* **55**, 17–32 (2012).
- 735 31. K. E. Clark, *et al.*, The hydrological regime of a forested tropical Andean catchment. *Hydrol.*
736 *Earth Syst. Sci.* **18**, 5377–5397 (2014).
- 737 32. M. A. Torres, Baronas J. Jotautas, Clark Kathryn E., Feakins Sarah J., West A. Joshua, Mixing as
738 a driver of temporal variations in river hydrochemistry: 1. Insights from conservative tracers in
739 the Andes-Amazon transition. *Water Resources Research* **53**, 3102–3119 (2017).
- 740 33. E. Burt, D. H. Coayla Rimachi, A. J. Ccahuana Quispe, A. J. West, Hydroclimate and bedrock
741 permeability determine young water fractions in streamflow across the tropical Andes mountains
742 and Amazon floodplain. *Hydrology and Earth System Sciences Discussions*, 1–27 (2022).
- 743 34. P. Vauchel, *et al.*, A reassessment of the suspended sediment load in the Madeira River basin from
744 the Andes of Peru and Bolivia to the Amazon River in Brazil, based on 10years of data from the
745 HYBAM monitoring programme. *Journal of Hydrology* **553**, 35–48 (2017).
- 746 35. J. J. Baronas, M. A. Torres, K. E. Clark, A. J. West, Mixing as a driver of temporal variations in
747 river hydrochemistry. Part 2: Major and trace element concentration dynamics in the Andes-
748 Amazon transition. *Water Resour. Res.*, n/a-n/a (2017).
- 749 36. E. I. Burt, *et al.*, Conservative transport of dissolved sulfate across the Rio Madre de Dios
750 floodplain in Peru. *Geology* (2021) <https://doi.org/10.1130/G48997.1> (May 19, 2021).
- 751 37. M. S. Wu, A. J. West, S. J. Feakins, Tropical soil profiles reveal the fate of plant wax biomarkers
752 during soil storage. *Organic Geochemistry* **128**, 1–15 (2019).
- 753 38. L. Märki, *et al.*, An unshakable carbon budget for the Himalaya. *Nat. Geosci.*, 1–6 (2021).
- 754 39. M. J. Bickle, E. Tipper, A. Galy, H. Chapman, N. Harris, On discrimination between carbonate
755 and silicate inputs to Himalayan rivers. *Am J Sci* **315**, 120–166 (2015).
- 756 40. L. Ghazi, M. Goñi, B. A. Haley, J. M. Muratli, J. C. Pett-Ridge, Concentration-runoff relationships
757 of contrasting small mountainous rivers in the Pacific Northwest, USA: Insights into the
758 weathering of rhenium relative to other weathering products. *Geochimica et Cosmochimica Acta*
759 **337**, 106–122 (2022).
- 760 41. W. Rahaman, S. K. Singh, A. D. Shukla, Rhenium in Indian rivers: Sources, fluxes, and
761 contribution to oceanic budget. *Geochem. Geophys. Geosyst.* **13**, Q08019 (2012).
- 762 42. C. A. Miller, B. Peucker-Ehrenbrink, B. D. Walker, F. Marcantonio, Re-assessing the surface
763 cycling of molybdenum and rhenium. *Geochimica et Cosmochimica Acta* **75**, 7146–7179 (2011).
- 764 43. J. Toma, *et al.*, Re-Os systematics and chronology of graphite. *Geochimica et Cosmochimica Acta*
765 **323**, 164–182 (2022).
- 766 44. A. Bufe, *et al.*, Co-variation of silicate, carbonate and sulfide weathering drives CO₂ release with
767 erosion. *Nature Geoscience* **14**, 211–216 (2021).
- 768 45. K. E. Clark, *et al.*, Storm-triggered landslides in the Peruvian Andes and implications for
769 topography, carbon cycles, and biodiversity. *Earth Surface Dynamics* **4**, 47–70 (2016).
- 770 46. M. A. Torres, *et al.*, Model predictions of long-lived storage of organic carbon in river deposits.
771 *Earth Surface Dynamics* **5**, 711–730 (2017).
- 772 47. J. A. Constantine, T. Dunne, J. Ahmed, C. Legleiter, E. D. Lazarus, Sediment supply as a driver
773 of river meandering and floodplain evolution in the Amazon Basin. *Nature Geoscience* (2014).
- 774 48. J. S. Scheingross, *et al.*, Preservation of organic carbon during active fluvial transport and particle

- 775 abrasion. *Geology* **47**, 958–962 (2019).
- 776 49. J. Gaillardet, B. Dupre, C. J. Allegre, P. Négrel, Chemical and physical denudation in the Amazon
777 River Basin. *Chemical Geology* **142**, 141–173 (1997).
- 778 50. M. Dellinger, R. G. Hilton, G. M. Nowell, Measurements of rhenium isotopic composition in low-
779 abundance samples. *J. Anal. At. Spectrom.* **35**, 377–387 (2020).
- 780 51. S. Moon, C. P. Chamberlain, G. E. Hilley, New estimates of silicate weathering rates and their
781 uncertainties in global rivers. *Geochimica et Cosmochimica Acta* **134**, 257–274 (2014).
- 782 52. N. Abastos Lara, “Balance hidrico superficial de la cuenca del rio Madre de Dios : Amazonia,
783 Bolivia, Peru” (PHICAB, 1987).
- 784 53. D. Colodner, *et al.*, The geochemical cycle of rhenium: a reconnaissance. *Earth and Planetary
785 Science Letters* **117**, 205–221 (1993).
- 786 54. A. Galy, C. France-Lanord, Weathering processes in the Ganges–Brahmaputra basin and the
787 riverine alkalinity budget. *Chemical Geology* **159**, 31–60 (1999).
- 788 55. D. G. Brookins, Rhenium as analog for fissionogenic technetium: Eh-pH diagram (25°C, 1 bar)
789 constraints. *Applied Geochemistry* **1**, 513–517 (1986).
- 790